



## OPEN ACCESS

## EDITED BY

Jianqiang Xu,  
Dalian University of Technology, China

## REVIEWED BY

Fabio Vivarelli,  
University of Bologna, Italy  
Himangshu Sonowal,  
University of California, San Diego,  
United States

## \*CORRESPONDENCE

Sue Lin,  
✉ iamkari@163.com  
Xiufeng Yan,  
✉ yanxiufeng@wzu.edu.cn

<sup>†</sup>These authors have contributed equally to this work and share first authorship

RECEIVED 23 October 2023

ACCEPTED 30 November 2023

PUBLISHED 13 December 2023

## CITATION

Zhang Y, Du J, Jin L, Pan L, Yan X and Lin S (2023), Iberverin exhibits antineoplastic activities against human hepatocellular carcinoma via DNA damage-mediated cell cycle arrest and mitochondrial-related apoptosis. *Front. Pharmacol.* 14:1326346. doi: 10.3389/fphar.2023.1326346

## COPYRIGHT

© 2023 Zhang, Du, Jin, Pan, Yan and Lin. This is an open-access article distributed under the terms of the [Creative Commons Attribution License \(CC BY\)](https://creativecommons.org/licenses/by/4.0/). The use, distribution or reproduction in other forums is permitted, provided the original author(s) and the copyright owner(s) are credited and that the original publication in this journal is cited, in accordance with accepted academic practice. No use, distribution or reproduction is permitted which does not comply with these terms.

# Iberverin exhibits antineoplastic activities against human hepatocellular carcinoma via DNA damage-mediated cell cycle arrest and mitochondrial-related apoptosis

Yuting Zhang<sup>1†</sup>, Jiao Du<sup>1†</sup>, Libo Jin<sup>2</sup>, Liying Pan<sup>1</sup>, Xiufeng Yan<sup>1,3\*</sup> and Sue Lin<sup>1,3\*</sup>

<sup>1</sup>College of Life and Environmental Science, Wenzhou University, Wenzhou, Zhejiang, China, <sup>2</sup>Institute of Life Sciences, Wenzhou University, Wenzhou, Zhejiang, China, <sup>3</sup>Zhejiang Provincial Key Laboratory for Water Environment and Marine Biological Resources Protection, Wenzhou University, Wenzhou, Zhejiang, China

Hepatocellular carcinoma (HCC) is one of the malignant tumors with high incidence and mortality rates in the world. Isothiocyanates (ITCs), bioactive substances present primarily in the plant order Brassicales, have been proved to be promising candidates for novel anti-HCC drugs with chemopreventive and anticancer activities. Iberverin, a predominant ITC isolated from the seeds of oxheart cabbage, has been discovered with anticancer property in lung cancer cells. However, the roles of iberverin in HCC remain elusive. In the present study, the effect and potential mechanisms of iberverin against human HCC were dissected. We demonstrated that low concentrations of iberverin inhibited cell proliferation, suppressed migration and induced mitochondrial-related apoptosis *in vitro*, and hampered tumorigenicity *in vivo*, with no obvious toxicity. Furthermore, we found that iberverin treatment induced DNA damage and G2/M phase arrest. Iberverin treatment also caused increased intracellular reactive oxygen species formation and glutathione depletion. Taken together, these results suggest that iberverin promotes mitochondrial-mediated apoptosis and induces DNA damage and G2/M cell cycle arrest in HCC by enhancing oxidative stress. Our findings provide better understanding of the anti-HCC mechanisms of ITCs and the potential for the natural product iberverin as a promising new anti-HCC biotherapeutic.

## KEYWORDS

hepatocellular carcinoma, iberverin, natural compound, antineoplastic activity, apoptosis, G2/M arrest

## 1 Introduction

Liver cancer is the sixth most common cancer and also the third leading cause of cancer-related deaths in the world, among which hepatocellular carcinoma (HCC) is the most common pathological type accounting for ~90% of cases (Llovet et al., 2016; Siegel et al., 2021; Sung et al., 2021). Considerable evidence demonstrates that the incidence of HCC is mostly associated with chronic liver disease, hepatitis virus B (HBV) and C (HCV) infection,

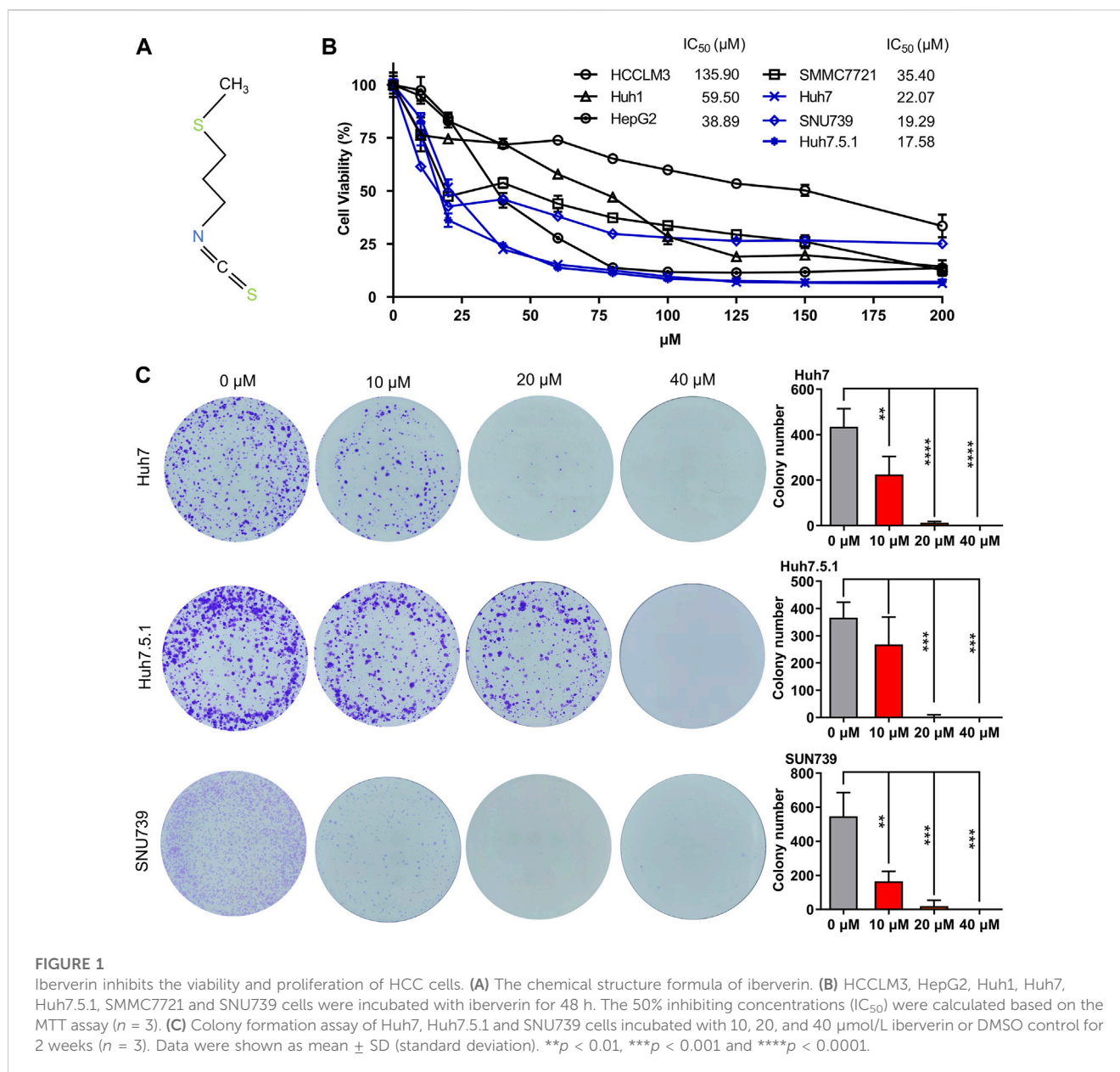


**FIGURE 1**

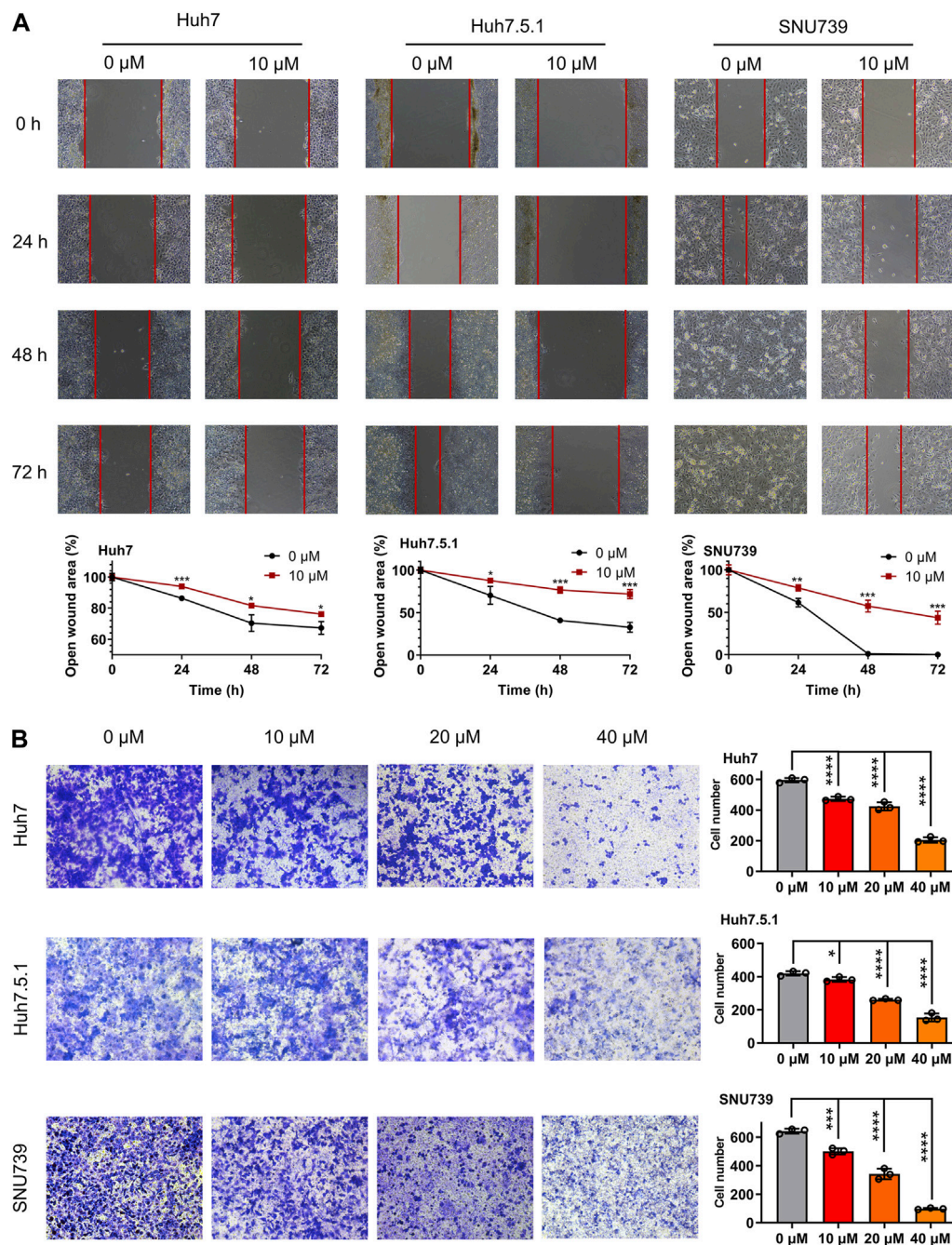
Iberverin inhibits the viability and proliferation of HCC cells. (A) The chemical structure formula of iberiverin. (B) HCCLM3, HepG2, Huh1, Huh7, Huh7.5.1, SMMC7721 and SNU739 cells were incubated with iberiverin for 48 h. The 50% inhibiting concentrations (IC<sub>50</sub>) were calculated based on the MTT assay ( $n = 3$ ). (C) Colony formation assay of Huh7, Huh7.5.1 and SNU739 cells incubated with 10, 20, and 40 μmol/L iberiverin or DMSO control for 2 weeks ( $n = 3$ ). Data were shown as mean  $\pm$  SD (standard deviation). \*\* $p < 0.01$ , \*\*\* $p < 0.001$  and \*\*\*\* $p < 0.0001$ .

and unhealthy drinking (Lin et al., 2013; Trinchet et al., 2015; Akinyemiju et al., 2017; Estes et al., 2018). Due to the relatively insidious onset and the lack of early screening, most HCC patients are frequently at advanced stages at the time of diagnosis and not eligible for curative surgery (Singh et al., 2014). For these patients, promising therapeutic strategies such as targeted drug therapy and systemic chemotherapy are the pivotal options. However, clinical application of these strategies, even treatments with sorafenib, lenvatinib or the combination of atezolizumab and bevacizumab, also cause some adverse reactions, such as elevated aspartate aminotransferase, hypertension and proteinuria (Llovet et al., 2021).

Biologically active natural compounds and their derivatives have drawn growing attention and have been confirmed as one of the most feasible solutions for hard-to-treat cancers (Dong et al., 2020; Fontana et al., 2020; Kubczak et al., 2021; Tewari et al., 2022). Isothiocyanates (ITCs) are hydrolysis products derived from glucosinolates, one of the plant secondary metabolites in the

order Brassicales (Nambiar et al., 2020). Accumulating evidence from encouraging *in vitro* and *in vivo* animal models indicates that several ITCs exert chemopreventive activity and inhibitory effects on multiple cancers, such as lung cancer, oral cancer and liver cancer (Rakariyatham et al., 2019; Boldry et al., 2020; Rekha et al., 2022; Zhang et al., 2022). Iberverin, namely, 3-methylthiopropyl ITC, is a predominant ITC in the seeds of oxheart cabbage (*Brassica oleracea* var. *capitata*) (Wang et al., 2010). It has been previously proved to possess anticancer properties in A549 lung carcinoma cells by promoting apoptosis through activation of Caspase-3, -8 and -9 (Wang et al., 2016). However, the potential roles of iberiverin in HCC and its molecular mechanism remain elusive.

In this study, *in vitro* and *in vivo* assays were performed to investigate the effect and potential mechanisms of iberiverin on HCC. It has been found that iberiverin could inhibit cell proliferation, suppress invasion and migration abilities, promote mitochondrial-related apoptosis, and arrest cell cycle in G2/M-phase arrest in HCC in



a dose-dependent manner. We demonstrated that iberverin-induced cell cycle arrest could be associated with DNA damage mediated by the induction of oxidative stress via accumulating reactive oxygen species (ROS) and consuming reduced glutathione (GSH). Meanwhile, iberverin could effectively inhibit the tumorigenic ability of HCC cells in mice with no obvious toxic effect on the body. These results suggest that the natural product iberverin has become a potentially promising new anti-HCC biotherapeutic.

## 2 Materials and methods

### 2.1 Cell lines and reagents

The human HCC cell lines HCCLM3, HepG2, Huh7, Huh7.5.1 and SMMC7721 were purchased from the China Typical Culture Collection Center (CCTCC), SNU739 from the Korean Cell Line Bank (KCLB), and Huh1 from the Japanese



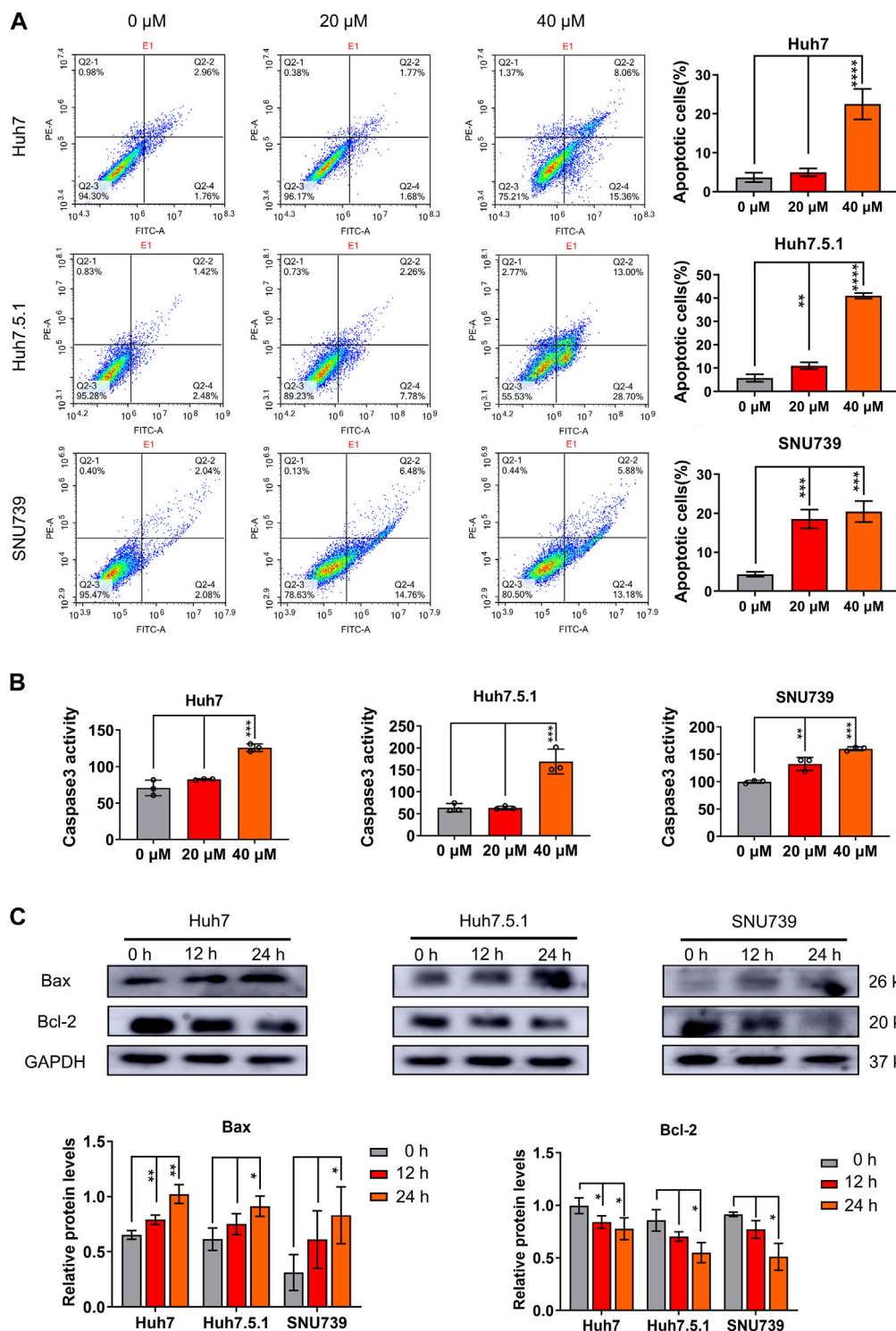


**FIGURE 3** Iberverin induces apoptosis in HCC cells. **(A)** Annexin V-FITC/PI double-staining assay by flow cytometry analysis of apoptosis in Huh7, Huh7.5.1 and SNU739 cells incubated with 20 and 40 μmol/L iberverin or DMSO control for 12 h. The percentage of apoptotic cells was shown on right panel ( $n = 3$ ). **(B)** Determination of Caspase-3 activity in Huh7, Huh7.5.1 and SNU739 cells incubated with 20 and 40 μmol/L iberverin or DMSO control for 12 h ( $n = 3$ ). **(C)** Western blot analysis of apoptotic proteins Bax and Bcl-2 in Huh7, Huh7.5.1 and SNU739 cells incubated with 20 μmol/L iberverin or DMSO control for 12 and 24 h. The histogram represented the expression levels of Bax and Bcl-2 proteins in three independent experiments ( $n = 3$ ). Data were shown as mean  $\pm$  SD. \* $p < 0.05$ , \*\* $p < 0.01$ , \*\*\* $p < 0.001$  and \*\*\*\* $p < 0.0001$ .

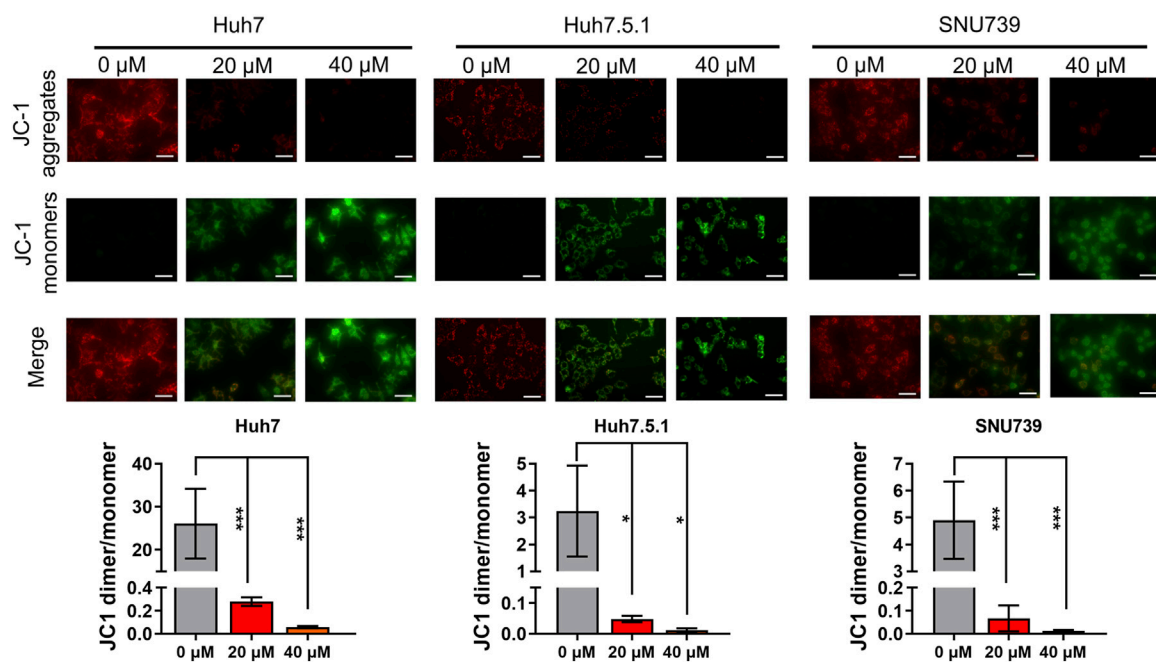


**FIGURE 4**

Iberberin causes decreased mitochondrial membrane potential (MMP) in HCC cells. JC-1-based immunofluorescence assay of Huh7, Huh7.5.1 and SNU739 cells incubated with 20 and 40  $\mu\text{mol/L}$  iberberin or DMSO control for 12 h ( $n = 3$ ). Red represents JC-1 aggregate signal, and green represent JC-1 monomer signal. The histogram represented the ratio of JC-1 aggregate/monomer in three independent experiments ( $n = 3$ ). Data were shown as mean  $\pm$  SD. \* $p < 0.05$  and \*\*\* $p < 0.001$ . Scale bars = 50  $\mu\text{m}$ .

Collection of Research Bioresources Cell Bank (JCRB). Cell lines HCCLM3, Huh1, Huh7, Huh7.5.1 and SMMC7721 were cultured in dulbecco's modified eagle medium (DMEM) (Gibco, the United States, catalog no. C11995500BT) supplemented with 10% fetal bovine serum (FBS) (Biological Industries, Israel, catalog no. 04-001-1ACS) and 1% v/v penicillin-streptomycin (Solarbio, P. R. China, catalog no. P1400). Cell lines SNU739 and HepG2 were cultured in RPMI 1640 medium (Gibco, the United States, catalog no. C11875500BT) and MEM (Procell, P. R. China, catalog no. PM150410), respectively, supplemented with 10% FBS and 1% v/v penicillin-streptomycin. Cells were incubated at 37°C with 5% CO<sub>2</sub>. All cell lines were negative for *mycoplasma* contamination.

Purified iberberin (>98%) was purchased from aladdin (Aladdin, P. R. China, catalog no. 505-79-3), dissolved in dimethyl sulfoxide (DMSO) (Solarbio, P. R. China, catalog no. D8371) to prepare a 500 mmol/L stock solution, and then stored in dark at -80°C.

## 2.2 MTT assay and colony formation assay

The antiproliferative effect of iberberin on human HCC cells was evaluated by MTT assay. HCCLM3, HepG2, Huh1, Huh7, Huh7.5.1, SMMC7721 and SNU739 cells were harvested and seeded in triplicate in a 96-well plate ( $5 \times 10^3$  cells per well) and incubated overnight. After 48 h of drug regimen treatments, 30  $\mu\text{L}$  of MTT solution (Solarbio, P. R. China, catalog no. 298-93-1) was added into each well. After 4 h of incubation at 37°C, the formazan crystals were dissolved in 150  $\mu\text{L}$  of DMSO, and the absorbance was measured at 490 nm with a microplate spectrometer (SPARK, Tecan, Swiss). The

half maximal inhibitory concentration (IC<sub>50</sub>) values were calculated using GraphPad Prism version 9.0.

For the colony formation assay, Huh7, Huh7.5.1 and SNU739 cells were seeded into a 6-well plate at a density of 5000 cells per well and incubated with 10, 20, and 40  $\mu\text{mol/L}$  iberberin or 0.1% DMSO control for 12 h. After incubation in fresh medium for 2 weeks, the cell colonies were washed twice with phosphate buffered solution (PBS) (Gibco, the United States, catalog no. C20012500BT), fixed with 4% paraformaldehyde (Biosharp, P. R. China, catalog no. BL539A) at room temperature for 15 min, washed three times with PBS, and stained with crystal violet (Beyotime, P. R. China, catalog no. C0121) for 15 min. The stained colonies were counted using ImageJ software.

## 2.3 Transwell invasion assay and wound healing migration assay

For wound healing migration assay, Huh7, Huh7.5.1 and SNU739 cells were seeded into 6-well plates ( $10^5$  cells per well). When cells reached 95%–100% confluence, a cell-free gap was created after scratching with a 10  $\mu\text{L}$  sterile pipette tip. After washing with PBS to remove detached cells, cells were treated with 10  $\mu\text{mol/L}$  iberberin or DMSO control for 12 h. At 0, 24, 48, and 72 h, the images were captured with a bright field microscope (Nikon, TS2-S-SM, Japan), and the migration distance was analyzed by ImageJ software.

For transwell invasion assay, Huh7, Huh7.5.1 and SNU739 cells were seeded into the upper chamber of 24-well transwell plates at a

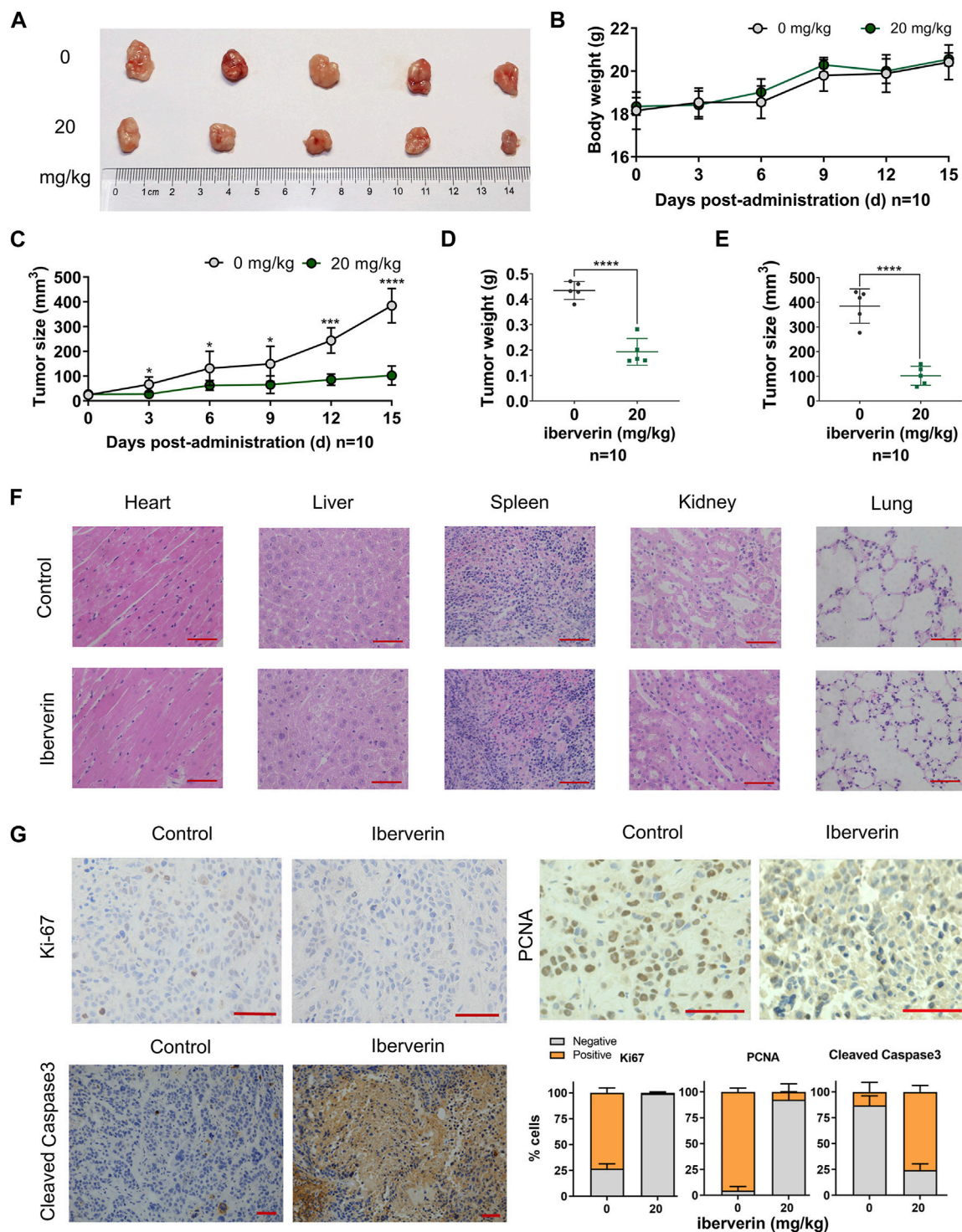
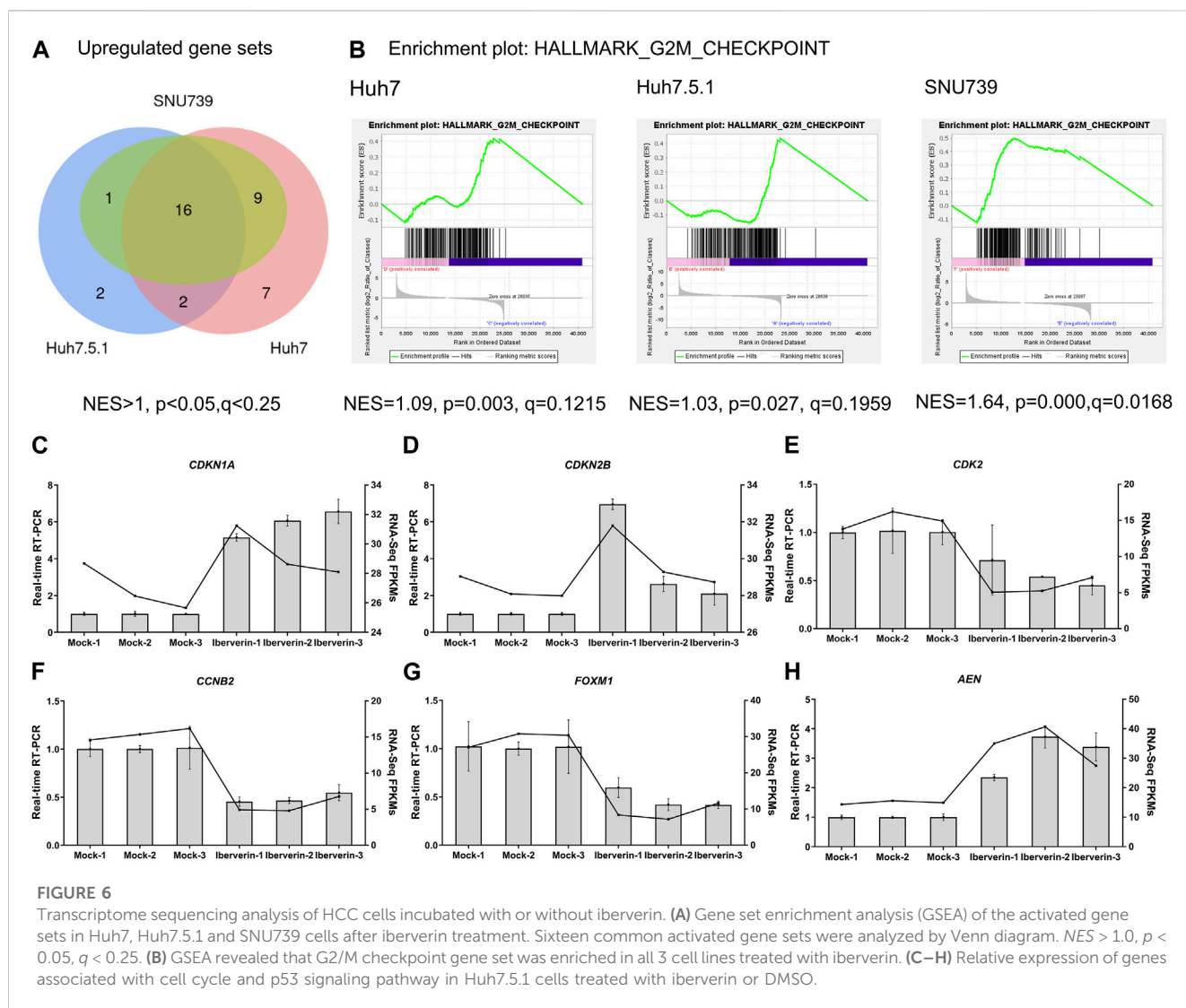


**FIGURE 5**

Iberverin inhibits the growth of Huh7.5.1 xenograft tumors in nude mice. (A) Huh7.5.1 xenograft tumors from the mice treated with iberiverin and DMSO, respectively ( $n = 10$ ). (B) The body weight of mice bearing Huh7.5.1 xenograft tumors measured every 3 days. (C) The growth curves of xenograft tumors. (D) and (E) The weight and size of Huh7.5.1 xenografts tumors calculated after executing the nude mice. (F) H&E stained tissue sections from mice treated with iberiverin and DMSO, respectively. (G) Representative IHC staining images of Ki-67, PCNA and cleaved Caspase-3 in Huh7.5.1 xenografts tumors from mice treated with iberiverin and DMSO, respectively. Data were shown as mean  $\pm$  SD. \* $p < 0.05$ , \*\*\* $p < 0.001$  and \*\*\*\* $p < 0.0001$ . Scale bars = 50  $\mu$ m.





density of  $2 \times 10^4$  cells per well, and 600  $\mu\text{L}$  of medium with 10% FBS was added to the lower chamber. After coculture with 10, 20 and 40  $\mu\text{mol/L}$  iberiverin or DMSO control for 12 h, cells that adhered to the lower surface were washed with PBS, fixed with 4% paraformaldehyde at room temperature for 15 min, washed three times with PBS, and stained with crystal violet for 15 min. The migrated cells on the lower surface were photographed with a bright field microscope (Nikon, TS2-S-SM, Japan).

## 2.4 Apoptosis assay by flow cytometry and TUNEL assay

Apoptosis assay was performed with a Annexin V-FITC/PI apoptosis detection kit (BD, the United States, catalog no. 556547) to measure iberiverin-induced apoptosis in HCC cells. Briefly, after incubation with 20 and 40  $\mu\text{mol/L}$  iberiverin or DMSO control for 12 h, Huh7, Huh7.5.1, and SNU739 cells were collected and washed twice with PBS. Then, cells were resuspended with 400  $\mu\text{L}$  of binding buffer, and stained with 5  $\mu\text{L}$  of Annexin V conjugated with fluorescein isothiocyanate (FITC) and 5  $\mu\text{L}$  of

propidium iodide (PI) solution to each sample. After incubation in dark for 15 min at room temperature, samples were analyzed by flow cytometry (FCM) (NovoCyte, Agilent, the United States).

A terminal deoxynucleotidyl transferase-mediated dUTP nick-end labeling (TUNEL) assay was conducted with a One Step TUNEL Apoptosis Assay Kit (Beyotime, P. R. China, catalog no. C1088) according to the manufacturer's instructions in conjunction with the DAPI staining to detect DNA fragmentation induced by iberiverin in HCC cells. In brief, Huh7, Huh7.5.1 and SNU739 cells were seeded in 6-well plates ( $10^4$  cells per well), cultured overnight, and then incubated with 20 and 40  $\mu\text{mol/L}$  iberiverin or DMSO control for 12 h. Subsequently, cells were washed with PBS and then fixed with 4% paraformaldehyde for 30 min. After infiltration with Triton X-100 (Beyotime, P. R. China, catalog no. P0096) for 5 min, cells were incubated with TUNEL reaction buffer for 30 min at 37°C in dark. The nuclei of cells were further stained with 10  $\mu\text{L}$  of 5 mg/L DAPI solution (BBI, P. R. China, catalog no. E607303) for 20 min in dark. Samples were observed under a fluorescence microscopy (Nikon, TS2-S-SM, Japan) to view the green fluorescence of apoptotic cells at 520 nm and blue DAPI-stained nuclei at 460 nm.

**TABLE 1** The gene sets significantly enriched in HCC cell lines after the treatment of iberiverin based on GSEA.

Cell lines	Hallmark gene set names	ES	NES	NOM p-val	FDR q-val
Huh7	HALLMARK_MYC_TARGETS_V2	0.55	1.37	0.001	0.1110
	HALLMARK_UNFOLDED_PROTEIN_RESPONSE	0.53	1.36	0.000	0.0630
	HALLMARK_TNFA_SIGNALING_VIA_NFKB	0.50	1.30	0.000	0.0654
	HALLMARK_MYC_TARGETS_V1	0.46	1.19	0.000	0.1223
	HALLMARK_OXIDATIVE_PHOSPHORYLATION	0.44	1.14	0.000	0.1428
	HALLMARK_REACTIVE_OXYGEN_SPECIES_PATHWAY	0.46	1.13	0.042	0.1300
	HALLMARK_PROTEIN_SECRETION	0.44	1.13	0.005	0.1147
	HALLMARK_MTORC1_SIGNALING	0.43	1.12	0.001	0.1096
	HALLMARK_G2M_CHECKPOINT	0.42	1.09	0.003	0.1215
	HALLMARK_CHOLESTEROL_HOMEOSTASIS	0.43	1.09	0.040	0.1121
	HALLMARK_INTERFERON_ALPHA_RESPONSE	0.42	1.08	0.025	0.1084
	HALLMARK_E2F_TARGETS	0.41	1.08	0.004	0.1039
	HALLMARK_APOPTOSIS	0.41	1.07	0.008	0.1001
	HALLMARK_APICAL_JUNCTION	0.41	1.07	0.005	0.0943
	HALLMARK_UV_RESPONSE_DN	0.41	1.07	0.007	0.0911
	HALLMARK_ADIPOGENESIS	0.41	1.07	0.002	0.0876
	HALLMARK_EPITHELIAL_MESENCHYMAL_TRANSITION	0.41	1.06	0.006	0.0982
	HALLMARK_KRAS_SIGNALING_UP	0.41	1.06	0.007	0.0960
	HALLMARK_INTERFERON_GAMMA_RESPONSE	0.41	1.06	0.006	0.0931
	HALLMARK_UV_RESPONSE_UP	0.41	1.05	0.019	0.0959
	HALLMARK_DNA_REPAIR	0.41	1.05	0.019	0.0923
	HALLMARK_ESTROGEN_RESPONSE_EARLY	0.40	1.05	0.007	0.0939
	HALLMARK_ESTROGEN_RESPONSE_LATE	0.40	1.05	0.016	0.0923
	HALLMARK_GLYCOLYSIS	0.40	1.05	0.008	0.0915
	HALLMARK_HYPOXIA	0.40	1.05	0.009	0.0886
	HALLMARK_FATTY_ACID_METABOLISM	0.40	1.04	0.028	0.0878
	HALLMARK_MYOGENESIS	0.40	1.04	0.016	0.0883
	HALLMARK_HEME_METABOLISM	0.40	1.04	0.017	0.0881
	HALLMARK_ALLOGRAFT_REJECTION	0.40	1.04	0.020	0.0885
	HALLMARK_P53_PATHWAY	0.40	1.04	0.016	0.0881
HALLMARK_IL2_STAT5_SIGNALING	0.40	1.03	0.034	0.1068	
HALLMARK_XENOBIOTIC_METABOLISM	0.40	1.03	0.039	0.1055	
HALLMARK_COMPLEMENT	0.40	1.03	0.036	0.1045	
HALLMARK_MITOTIC_SPINDLE	0.39	1.02	0.049	0.1234	
Huh7.5.1	HALLMARK_TNFA_SIGNALING_VIA_NFKB	0.60	1.42	0.000	0.0475
	HALLMARK_INFLAMMATORY_RESPONSE	0.52	1.23	0.000	0.1355
	HALLMARK_TGF_BETA_SIGNALING	0.50	1.13	0.041	0.2320
	HALLMARK_MYC_TARGETS_V2	0.49	1.12	0.040	0.1908

(Continued on following page)



**TABLE 1 (Continued)** The gene sets significantly enriched in HCC cell lines after the treatment of iberiverin based on GSEA.

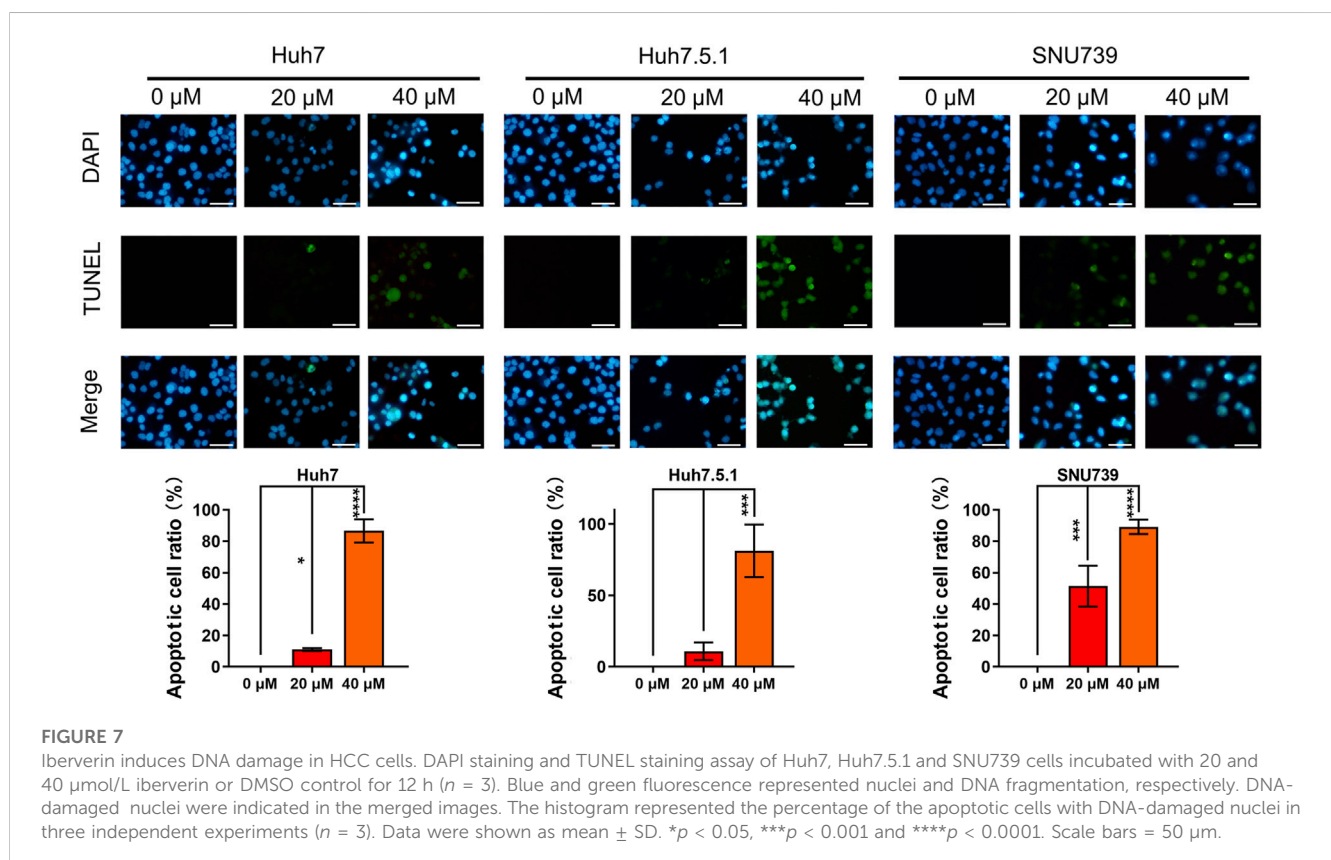
Cell lines	Hallmark gene set names	ES	NES	NOM p-val	FDR q-val
	HALLMARK_EPITHELIAL_MESENCHYMAL_TRANSITION	0.47	1.11	0.001	0.1635
	HALLMARK_MYC_TARGETS_V1	0.46	1.09	0.001	0.1725
	HALLMARK_DNA_REPAIR	0.46	1.09	0.007	0.1605
	HALLMARK_MTORC1_SIGNALING	0.46	1.08	0.001	0.1497
	HALLMARK_OXIDATIVE_PHOSPHORYLATION	0.45	1.06	0.002	0.1713
	HALLMARK_BILE_ACID_METABOLISM	0.45	1.05	0.043	0.1910
	HALLMARK_HYPOXIA	0.44	1.05	0.010	0.1980
	HALLMARK_ESTROGEN_RESPONSE_EARLY	0.44	1.04	0.015	0.2143
	HALLMARK_MYOGENESIS	0.44	1.04	0.020	0.1971
	HALLMARK_APICAL_JUNCTION	0.44	1.03	0.021	0.1897
	HALLMARK_G2M_CHECKPOINT	0.44	1.03	0.027	0.1959
	HALLMARK_E2F_TARGETS	0.44	1.03	0.032	0.1787
	HALLMARK_APOPTOSIS	0.44	1.03	0.048	0.1743
	HALLMARK_ADIPOGENESIS	0.44	1.03	0.032	0.1723
	HALLMARK_IL2_STAT5_SIGNALING	0.44	1.03	0.040	0.1673
	HALLMARK_P53_PATHWAY	0.44	1.03	0.044	0.1687
	HALLMARK_HEME_METABOLISM	0.43	1.02	0.048	0.1797
SNU739	HALLMARK_MYC_TARGETS_V2	0.65	2.01	0.000	0.0010
	HALLMARK_TNFA_SIGNALING_VIA_NFKB	0.57	1.88	0.000	0.0025
	HALLMARK_G2M_CHECKPOINT	0.50	1.64	0.000	0.0168
	HALLMARK_MYC_TARGETS_V1	0.45	1.49	0.000	0.0375
	HALLMARK_PROTEIN_SECRETION	0.46	1.47	0.004	0.0354
	HALLMARK_TGF_BETA_SIGNALING	0.44	1.35	0.021	0.0622
	HALLMARK_OXIDATIVE_PHOSPHORYLATION	0.40	1.33	0.001	0.0605
	HALLMARK_REACTIVE_OXYGEN_SPECIES_PATHWAY	0.42	1.30	0.040	0.0629
	HALLMARK_E2F_TARGETS	0.39	1.28	0.000	0.0620
	HALLMARK_UNFOLDED_PROTEIN_RESPONSE	0.39	1.27	0.004	0.0619
	HALLMARK_ADIPOGENESIS	0.36	1.18	0.003	0.0969
	HALLMARK_P53_PATHWAY	0.35	1.16	0.000	0.0974
	HALLMARK_HYPOXIA	0.35	1.14	0.002	0.0994
	HALLMARK_MITOTIC_SPINDLE	0.35	1.14	0.003	0.0978
	HALLMARK_EPITHELIAL_MESENCHYMAL_TRANSITION	0.34	1.13	0.003	0.0948
	HALLMARK_MTORC1_SIGNALING	0.34	1.13	0.003	0.0942
	HALLMARK_APICAL_JUNCTION	0.34	1.10	0.003	0.1079
	HALLMARK_UV_RESPONSE_DN	0.34	1.10	0.018	0.1022
	HALLMARK_GLYCOLYSIS	0.33	1.10	0.004	0.1014
	HALLMARK_UV_RESPONSE_UP	0.33	1.09	0.025	0.1059
	HALLMARK_KRAS_SIGNALING_UP	0.33	1.08	0.013	0.1002

(Continued on following page)

TABLE 1 (Continued) The gene sets significantly enriched in HCC cell lines after the treatment of iberiverin based on GSEA.

Cell lines	Hallmark gene set names	ES	NES	NOM p-val	FDR q-val
	HALLMARK_DNA_REPAIR	0.33	1.06	0.029	0.1073
	HALLMARK_IL2_STAT5_SIGNALING	0.32	1.06	0.021	0.1122
	HALLMARK_MYOGENESIS	0.32	1.05	0.030	0.1147
	HALLMARK_HEME_METABOLISM	0.32	1.04	0.022	0.1196
	HALLMARK_XENOBIOTIC_METABOLISM	0.31	1.03	0.043	0.1461

NES >1, NOM p-val <0.05, FDR q-val <0.25.



## 2.5 Detection of Caspase-3 activity

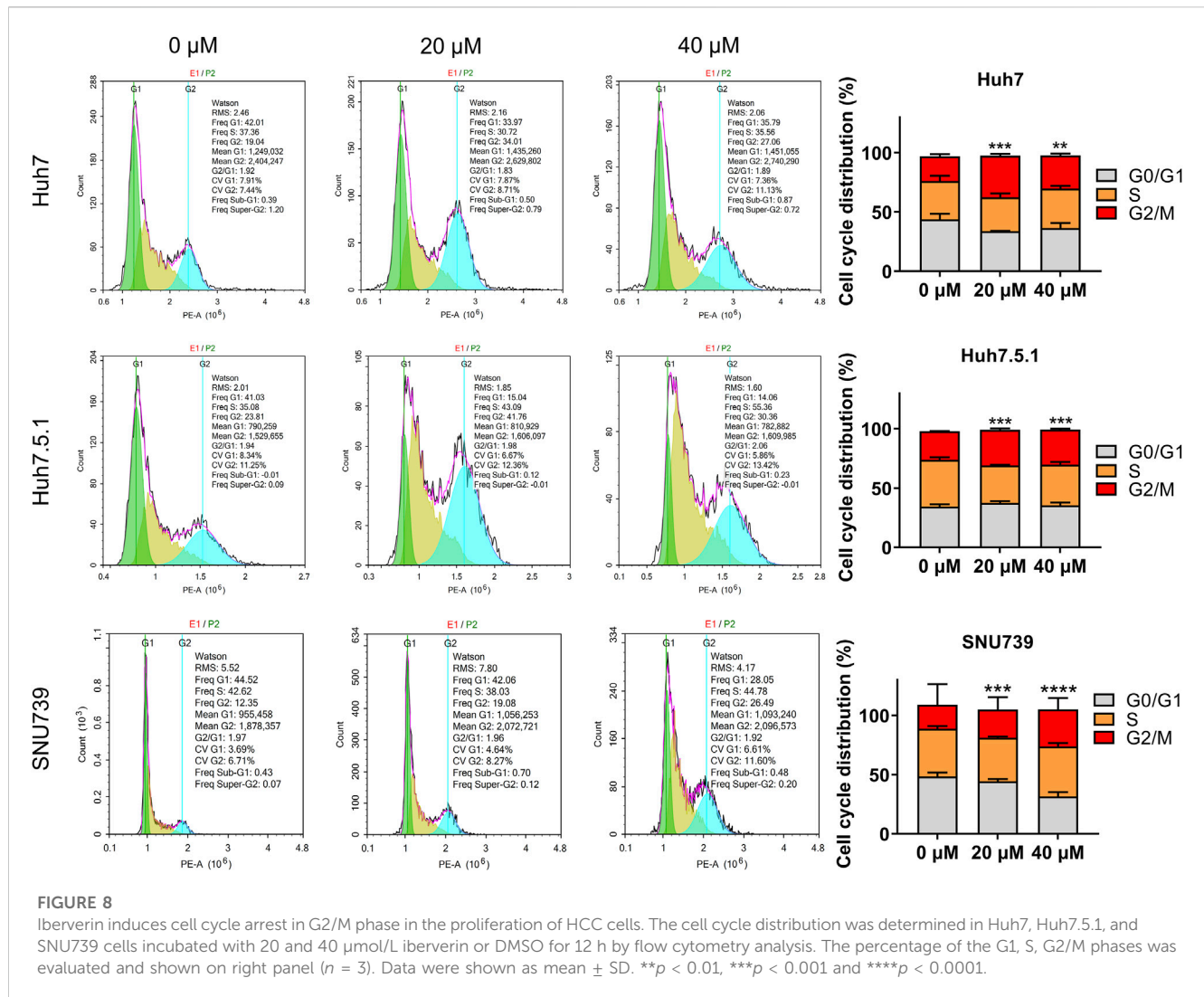
Huh7, Huh7.5.1 and SNU739 cells were seeded into 6-well plates at a density of  $10^5$  cells per well and cultured overnight. After incubation with 20 and 40 μmol/L iberiverin or DMSO control for 12 h, Caspase-3 enzymatic activity level was measured via the detection of *p*-nitroaniline (*p*NA) cleavage by Caspase-3-specific substrates using a Caspase-3 assay kit (Beyotime, P. R. China, catalog no. C1116). According to the manufacturer's instructions, cells were collected, lysed and then centrifuged at  $20,000 \times g$  for 15 min at 4°C in a precooled centrifuge. The enzymatic reaction for Caspase-3 activity was performed at 37°C for 2 h with 50 μL of cell lysate, 40 μL of reaction buffer and 10 μL of Caspase-3 colorimetric substrate (acetyl-Asp-Glu-Val-Asp *p*-nitroanilide, Ac-DEVD-*p*NA) in each reaction. The color intensity of *p*NA was measured at 405 nm with a microplate spectrometer (SPARK, Tecan, Swiss).

## 2.6 Determination of mitochondrial membrane potential

Huh7, Huh7.5.1 and SNU739 cells were seeded into 6-well plates ( $10^5$  cells per well) and cultured overnight. After incubation with 20 and 40 μmol/L iberiverin or DMSO control for 12 h, cells were collected and washed with PBS. The changes in mitochondrial membrane potential (MMP) were detected using the JC-1 Assay Kit (Beyotime, P. R. China, catalog no. C2006) under a fluorescence microscopy (Nikon, TS2-S-SM, Japan) as described in the product manual.

## 2.7 Cell cycle analysis

Huh7, Huh7.5.1 and SNU739 cells were seeded into 6-well plates ( $10^5$  cells per well) and cultured overnight. After incubation with



20 and 40 μmol/L iverberin or DMSO control for 12 h, cells were harvested, washed twice with precooled PBS and stored in 75% ethanol at  $-20^{\circ}\text{C}$  overnight. For PI/RNase staining, overnight-fixed cells were resuspended with 500 μL of PI/RNase Staining Buffer (BD, the United States, catalog no. 550825). After incubation away from light for 15 min at room temperature, samples were analyzed by FCM.

## 2.8 Western blotting and antibodies

After treatment with 20 μmol/L iverberin, the total cellular protein was extracted using the RIPA lysis buffer (Boster, P. R. China, catalog no. AR0103) and separated by 12.5% SDS-PAGE gel (YEASEN, P.R. China, catalog no. 20326ES62). Target protein was then transferred from the SDS-PAGE gel to a PVDF membrane (Merck Millipore, the United States, catalog no. IPVH00010) followed by blocking with 5% skim milk (Solarbio, P. R. China, catalog no. LP0033B). The membranes were incubated overnight at  $4^{\circ}\text{C}$  with the corresponding primary antibodies, washed, and then incubated

with the proper secondary antibodies. GAPDH was used for normalization. Anti-Bax (CST, the United States, catalog no. 2772S) and anti-GAPDH (CST, the United States, catalog no. 2118S) were purchased from Cell Signaling Technology (Beverly, MA, the United States). Anti-Bcl-2 (BBI, P. R. China, catalog no. D151534) was purchased from BBI (China).

## 2.9 Determination of oxidative stress and antioxidant defenses

Huh7, Huh7.5.1, and SNU739 cells were seeded into 6-well plates and cultured overnight. After incubation with 20 and 40 μmol/L iverberin or DMSO control for 12 h, cells were harvested. For ROS assay, the oxidation-sensitive fluorescent probe DCFH-DA (Beyotime, P. R. China, catalog no. S0033S) was used to detect intracellular ROS levels according to the instructions by FCM. For quantification of GSH, a GSH assay kit (Solarbio, P. R. China, catalog no. BC1175) was used according to the manufacturer's instructions. The GSH concentration was normalized to the cell number.



TABLE 2 The core enrichment genes of hallmark G2M CHECKPOINT gene set in HCC cell lines treated with iberiverin based on GSEA.

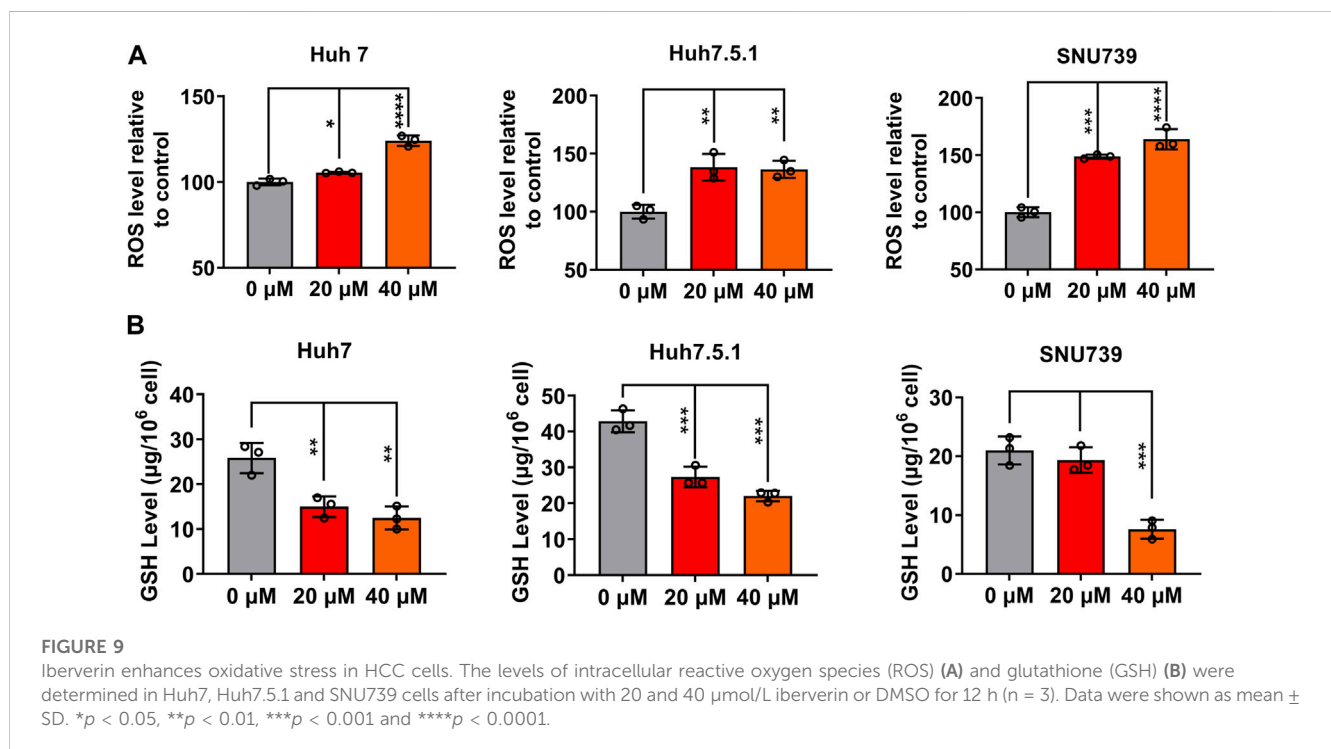
Cell lines	Genes <sup>a</sup>	Rank metric scores	Running ES	Core enrichment
Huh7	<i>HUS1</i> *	0.674280345	-0.066083774	Yes
	<i>CDC25A</i> *	0.54730624	-0.021954276	Yes
	<i>H2BC12</i>	0.397074491	0.007916474	Yes
	<i>CDC6</i> *	0.246321559	0.03360164	Yes
	<i>ORC6</i> *	0.231656134	0.035954203	Yes
	<i>DBF4</i> *	0.189768985	0.0422332	Yes
	<i>EXO1</i> *	0.116855599	0.047004547	Yes
	<i>RPA2</i> *	0.054428279	0.038238443	Yes
	<i>ORC5</i> *	0.030267492	0.031266432	Yes
	<i>MCM6</i> *	-0.037066828	-0.002669783	Yes
	<i>CHEK1</i> *	-0.096802443	-0.013186244	Yes
	<i>MCM2</i>	-0.223403722	0.007531589	Yes
	<i>NSD2</i>	-0.247092977	0.014205299	Yes
	<i>MCM5</i>	-0.358161062	0.079927996	Yes
	<i>CDC7</i> *	-0.361887842	0.0952116	Yes
	<i>MCM3</i> *	-0.531770051	0.21273686	Yes
	<i>CCNB2</i>	-0.537943661	0.22775517	Yes
	<i>WRN</i> *	-0.545878589	0.2426727	Yes
	<i>CDK1</i> *	-0.618214726	0.28907275	Yes
	<i>CDC45</i>	-0.691384554	0.3269976	Yes
<i>BARD1</i>	-0.762358725	0.38143694	Yes	
Huh7.5.1	<i>HUS1</i> *	0.660314441	-0.09981071	Yes
	<i>CDC25A</i> *	0.376548588	-0.070587374	Yes
	<i>ORC6</i> *	0.309317529	-0.06927699	Yes
	<i>WRN</i> *	0.283825129	-0.07110837	Yes
	<i>CDC6</i> *	-0.005761847	-0.11234292	Yes
	<i>CHEK1</i> *	-0.058090433	-0.12541598	Yes
	<i>MCM5</i>	-0.141590282	-0.13823974	Yes
	<i>DBF4</i> *	-0.162432313	-0.13973919	Yes
	<i>RPA2</i> *	-0.450888664	-0.1486315	Yes
	<i>EXO1</i> *	-0.461915255	-0.1434403	Yes
	<i>ORC5</i> *	-0.481425107	-0.14327826	Yes
	<i>MCM2</i>	-0.571308434	-0.12855072	Yes
	<i>NSD2</i>	-0.627520025	-0.09856759	Yes
	<i>CDC45</i>	-0.662444711	-0.09363544	Yes
	<i>H2BC12</i>	-0.698840201	-0.060440045	Yes
	<i>MCM3</i> *	-0.786862969	-0.017804312	Yes
	<i>MCM6</i> *	-0.997158408	0.08679963	Yes

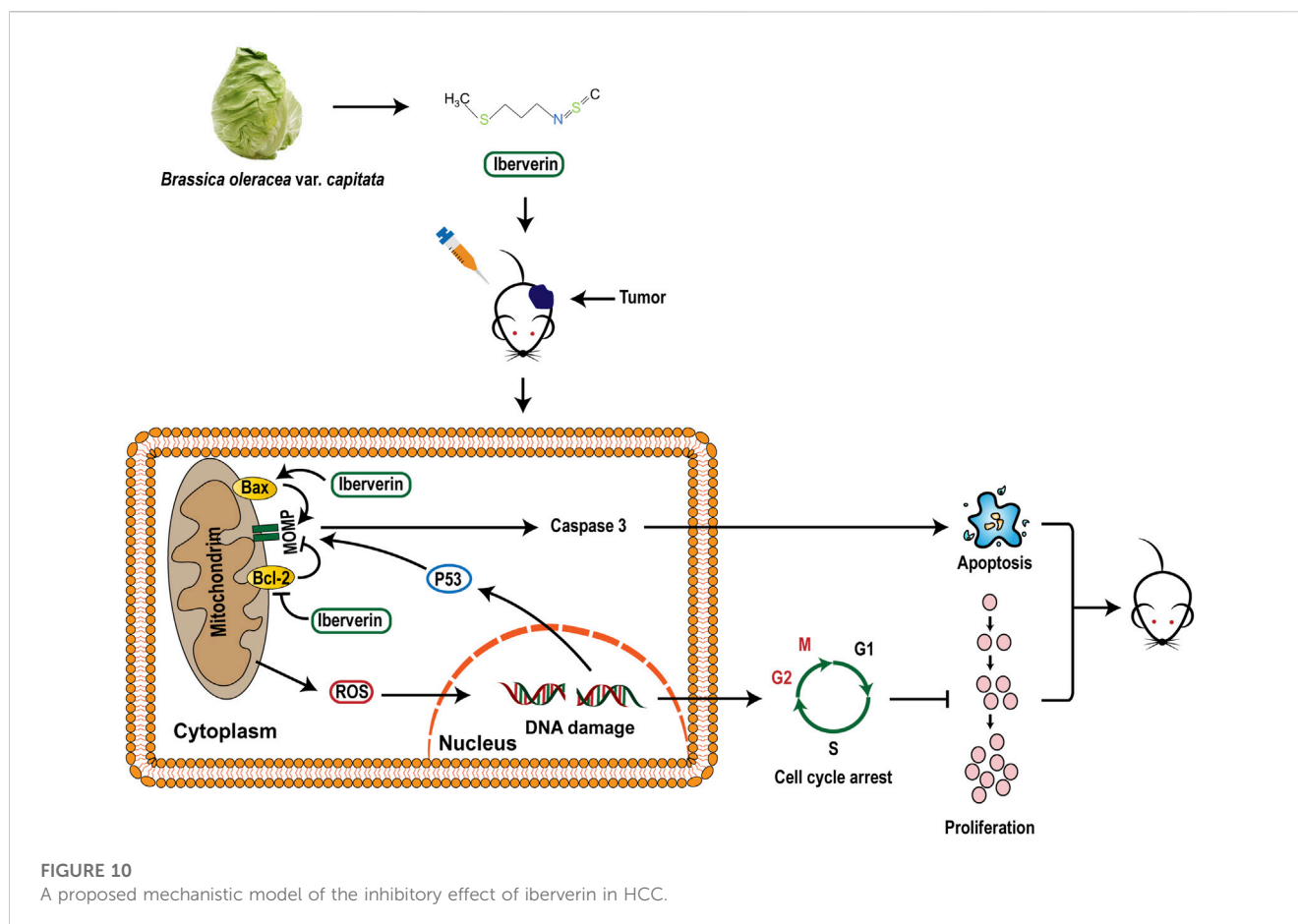
(Continued on following page)

**TABLE 2 (Continued)** The core enrichment genes of hallmark G2M CHECKPOINT gene set in HCC cell lines treated with iberberin based on GSEA.

Cell lines	Genes <sup>a</sup>	Rank metric scores	Running ES	Core enrichment
	<i>CDK1</i> *	-1.127957225	0.11787925	Yes
	<i>BARD1</i>	-1.247657418	0.21405476	Yes
	<i>CDC7</i> *	-1.470173478	0.26555622	Yes
	<i>CCNB2</i>	-1.603772998	0.30941218	Yes
SNU739	<i>WRN</i> *	0.505983651	0.0102293	Yes
	<i>ORC5</i> *	0.497382909	0.040960204	Yes
	<i>DBF4</i> *	0.401874721	0.088307604	Yes
	<i>CDC25A</i> *	0.346485287	0.15242542	Yes
	<i>CDC6</i> *	0.332688808	0.17050894	Yes
	<i>RPA2</i> *	0.306001008	0.20940134	Yes
	<i>ORC6</i> *	0.299213856	0.22673178	Yes
	<i>EXO1</i> *	0.282092005	0.27787817	Yes
	<i>HUS1</i> *	0.270357847	0.30350763	Yes
	<i>CHEK1</i> *	0.269389927	0.30905035	Yes
	<i>CDK1</i> *	0.252586246	0.31889796	Yes
	<i>MCM3</i> *	0.189492613	0.4019202	Yes
	<i>CDC7</i> *	0.16343157	0.4360845	Yes
	<i>MCM6</i> *	0.13451378	0.46395138	Yes

<sup>a</sup>Fourteen common core enrichment genes that are present in all three HCC cell lines and associated with G2/M checkpoint based on Reactome pathway analysis are indicated by asterisks.





## 2.10 Nude mice xenograft assay

A total of ten immunodeficient BALB/c nude female mice (4–6 weeks-old) purchased from Hangzhou Medical College were randomly divided into two groups with five mice in each group and allowed to adapt for 1 week prior to the experiment. Huh7.5.1 cells ( $1 \times 10^7$ ) were implanted into the back of mice by subcutaneous injection. At 7 days after implantation, mice were treated as follows: 1) control group, 50  $\mu$ L of DMSO, intraperitoneal injection; 2) 20 mg/kg iberiverin dissolved in DMSO, intraperitoneal injection. The treatment regimens were administered every 3 days for five cycles, and the tumor size and the body weight of mice were measured every 3 days. After the animals were sacrificed under anesthesia, the tumor tissues were removed and weighted. The tumor volume calculation formula was as follows:  $V = 0.5 \times \text{length} \times \text{width}^2$ . All animal procedures were in accordance with the guidelines of the Animal Policy and Welfare Committee of Wenzhou University.

## 2.11 Histopathology and immunohistochemistry staining

Tissue samples were fixed with 4% paraformaldehyde, embedded in paraffin, and cut into 4  $\mu$ m sections. Paraffin sections of organs were stained with hematoxylin-eosin (H&E) staining for routine histological examination and morphometric

analysis. For immunohistochemistry (IHC) staining, tumor sections were deparaffinized with xylene and gradually rehydrated with ethanol, followed by incubation in 3% hydrogen peroxide to block the endogenous peroxidase activity. After heat-mediated antigen retrieval, the slides were blocked with 10% normal goat serum for 15 min, and then incubated with anti-Ki-67 (Abcam, the United Kingdom, catalog no. ab16667), anti-PCNA (Proteintech, the United States, catalog no. 10205-2-AP) and anti-Cleaved Caspase-3 (Cell Signaling, the United States, catalog no. 9661s) antibodies, respectively, at 4°C overnight. The sections were washed with PBS and incubated with the secondary antibodies at room temperature for 1 h, followed by detection using a DAB kit (DAKO, Denmark, catalog no. K5007) and examination by light microscopy.

## 2.12 RNA-seq and data analysis

A total of 1  $\mu$ g RNA was isolated from Huh7, Huh7.5.1 and SNU739 cells treated with 20  $\mu$ mol/L iberiverin or DMSO control for 12 h, respectively, and then enriched with polyA<sup>+</sup> using Dynabeads Oligo (dT) magnetic beads (Thermo Fisher, the United States, catalog no. 25-61005). The polyA<sup>+</sup> RNA was used as input material for library preparations using a NEBNext<sup>®</sup> Magnesium RNA Fragmentation Module (NEB, the United States, catalog no. E6150S). Subsequently, paired-end sequencing was performed on Illumina Novaseq<sup>™</sup> 6000 by LC-Bio Technology Co., Ltd. (Hangzhou, China). Gene expression abundance was showed by



Fragments per Kilobase of Transcript per Million mapped reads (FPKM). Gene Set Enrichment Analysis (GSEA) was performed for gene functional annotation.

### 2.13 Real-time RT-PCR analysis

Residual RNA samples for RNA-seq were transcribed into cDNA using a PrimeScript™ RT reagent kit with gDNA Eraser (TAKARA, Japan, catalog no. RR047A). *GAPDH* was used as the normalization control. Real-time RT-PCR was performed on a BioRad CFX Connet Real-time RT-PCR Detection system (BioRad, the United States) and the relative expression levels were analyzed. All primers used were listed in Supplementary Table S1.

### 2.14 Statistical analysis

Statistical differences between groups were determined using *t*-test or one-way ANOVA using GraphPad Prism version 9.0. *p*-values <0.05 were considered statistically significant.

## 3 Results

### 3.1 Iberverin inhibits the viability and proliferation of HCC cells *in vitro*

In order to demonstrate the broad inhibitory effect of iberberin (Figure 1A) on different HCC cells, seven HCC cell lines, HCCLM3, HepG2, Huh1, Huh7, Huh7.5.1, SMMC7721 and SNU739 were employed. For a short-term study, HCC cells were treated with the indicated concentration of iberberin and DMSO for 48 h, respectively, and then subjected to the MTT assay. Generally, the antiproliferative effect of iberberin on HCC cells was positively correlated to the dose of iberberin (Figure 1B). Among these HCC cell lines, Huh7, Huh7.5.1, and SNU739 were most sensitive to iberberin with  $IC_{50}$  less than 25  $\mu\text{mol/L}$ , followed by SMMC7721 and Huh1 with  $IC_{50}$  between 50 and 100  $\mu\text{mol/L}$  (Figure 1B). Therefore, Huh7, Huh7.5.1, and SNU739 cell lines, on which iberberin exerted a relatively strong inhibitory effect, were chosen for further study. As expected, clonogenic survival rate of Huh7, Huh7.5.1 and SNU739 cells was significantly decreased in a dose-dependent manner after iberberin treatment, as indicated by the significant reduction of colony numbers and sizes (Figure 1C).

### 3.2 Iberverin suppresses the migration and invasion of HCC cells

In order to investigate whether iberberin could impair the migration of HCC cells, wound healing migration assay was conducted. After treatment with 10  $\mu\text{mol/L}$  iberberin, the migration rate of Huh7, Huh7.5.1 and SNU739 cells was remarkably delayed compared with the control group (Figure 2A). Consistent with the result of wound healing migration assay, the invasive ability of Huh7, Huh7.5.1 and

SNU739 cells was markedly suppressed in a dose-dependent manner (Figure 2B).

### 3.3 Iberverin induces mitochondrial-related apoptosis in HCC cells

To evaluate the role of apoptosis in the growth-inhibitory effects of iberberin in HCC cells, the apoptotic cell death induced by iberberin was characterized by FCM with Annexin V-FITC/PI staining. The number of apoptotic cells in Huh7, Huh7.5.1 and SNU739 cells increased significantly by 7.4, 7.1 and 4.7 times after treatment with 40  $\mu\text{mol/L}$  iberberin, respectively, compared with control cells (Figure 3A). Meanwhile, the effects of iberberin in apoptosis induction of HCC cells is dose-dependent (Figure 3A). Subsequently, a substantial increase in Caspase-3 activity in Huh7, Huh7.5.1 and SNU739 cells was determined after co-incubation with iberberin (Figure 3B). Furthermore, Western blot analysis provided additional supportive evidence, revealing that iberberin enhanced the level of apoptotic protein Bax but repressed the expression of Bcl-2 in Huh7, Huh7.5.1 and SNU739 cells in a time-dependent manner (Figure 3C), confirming the pro-apoptotic effect of iberberin *in vitro*.

As mitochondrial-related apoptosis is triggered by Bcl-2 family-mediated mitochondrial outer membrane permeabilization (MOMP), which subsequently activates caspase proteases and ultimately promotes cell self-destruction (Liu et al., 2018), thus, we further determined the changes in MMP. Immunofluorescence assay showed a significant decrease of MMP in all three HCC cell lines treated with iberberin, as indicated by the reduction in the red JC-1 aggregate signal and simultaneously the increase in the green fluorescence intensity (Figure 4).

### 3.4 Iberverin suppresses the growth of HCC xenograft tumors

To determine the antineoplastic potential of iberberin on HCC *in vivo*, Huh7.5.1 cells were subcutaneously injected into immunodeficient BALB/c nude mice to generate xenograft tumors. These mice were randomly divided into two groups and further subjected to drug regimes. Compared with control group, the marked reduction in the size by 73.4% and weight by 55.3% of Huh7.5.1 xenograft tumors treated with iberberin was detected, respectively (Figures 5A,C–E). However, the body weight of the two groups of mice gradually increased, without significant difference between each other (Figure 5B). In addition, H&E staining of tissue sections (heart, liver, spleen, kidney and lung) from the mice bearing Huh7.5.1 xenograft tumors was also consistent with this observation, exhibiting no obvious histological changes (Figure 5F). These findings confirm that iberberin exerts notably antineoplastic activity against HCC but possesses no systematic toxicity.

To further assess the antiproliferative and pro-apoptotic effect of iberberin on HCC *in vivo*, the expression of Ki-67 and PCNA (two proliferation markers) and cleaved Caspase-3 (an apoptosis marker) in xenograft tumors was investigated by IHC staining. As shown in Figure 5G, both Ki-67 and PCNA were significantly decreased in

iberberin-treated Huh7.5.1 xenograft tumors, whereas cleaved Caspase-3 was remarkably increased, suggesting that iberberin could inhibit tumor growth of HCC by suppressing cell proliferation and promoting cell apoptosis *in vivo*.

### 3.5 Transcriptome assay suggests that iberberin activates the G2/M checkpoint and p53 pathway in HCC cells

To further delineate the potential molecular mechanisms underlying the effects of iberberin on HCC, the transcriptome sequencing was conducted to assess the genome-wide effect of iberberin on gene expression in Huh7, Huh7.5.1 and SNU739 cells incubated with iberberin and DMSO, respectively (Supplementary Table S2). GSEA analysis showed that sixteen gene sets were significantly enriched in the iberberin-upregulated transcripts in all 3 cell lines, including genes associated with the G2/M checkpoint, DNA repair and the p53 signaling pathway (Figures 6A,B; Table 1).

Real-time RT-PCR further confirmed that the expression levels of the cell cycle genes, *CDKN1A*, *CDKN2B*, *CDK2*, *CCNB2*, and *FOXM1*, were dysregulated in Huh7.5.1 cells following iberberin exposure (Figures 6C–G). In addition, the expression of *AEN*, which is targeted and induced by p53 and required for efficient DNA fragmentation in p53-dependent apoptosis (Kawase et al., 2008), was also enhanced after iberberin treatment (Figure 6H). These results showed that the cell cycle- and p53-related gene sets could be activated by iberberin, and G2/M DNA damage checkpoint might be a key tumor suppressor checkpoint, indicating the potential regulatory mechanisms of iberberin in terms of its anti-HCC effect.

### 3.6 Iberberin-induced DNA damage causes G2/M cell cycle arrest in a ROS-dependent manner in HCC cells

Based on GESA, DNA repair gene set was significantly enriched in all 3 cell lines (Table 1), indicating that iberberin might induce DNA damage. As DNA damage, most often involving large DNA fragmentation, is widely observed in dying cells that display apoptotic morphological changes (Kaufmann et al., 2000), a DAPI staining and TUNEL staining assay was conducted to examine iberberin-induced DNA damage in HCC cells. It was revealed that iberberin induced a marked increase of green fluorescence in HCC cells in a dose-dependent manner (Figure 7), indicating the occurrence of DNA damage in the nuclei. What was more, when treated with iberberin at a concentration of 40  $\mu\text{mol/L}$ , a large number of nuclei had broken down, as reflected by the DAPI staining (Figure 7). These results clearly indicated that iberberin exposure induced DNA damage in HCC cells.

As DNA damage can cause cell cycle arrest, we further investigated the implication of iberberin in cell cycle distribution through PI/RNase staining by FCM analysis. The result revealed that iberberin obviously induced G2/M cell cycle arrest in Huh7, Huh7.5.1 and SNU739 cells, whereas reduced the population of

cells in G1 and S phases (Figure 8). Moreover, the core enrichment genes for the activated G2/M checkpoint from GSEA were further investigated based on Reactome pathway analysis, and fourteen genes were finally identified in all 3 cell lines (Table 2). In this study, p53 pathway, which has been demonstrated to be enhanced by DNA damage and regulate the cell cycle progression (Helton and Chen, 2007; Engeland, 2022), was also activated based on GSEA (Table 1). All these results suggested that the inhibitory roles of iberberin in the growth of HCC cells could be attributed to G2/M arrest caused by DNA damage.

ROS accumulation and GSH depletion that have been found to promote cancer cell death are crucial events in oxidative stress (Arfin et al., 2021). They have been shown to mediate DNA damage, checkpoint responses, and apoptosis in diverse cancers (Barzilai and Yamamoto, 2004; Guachalla and Rudolph, 2010; Guo et al., 2014; Sadiq, 2023). Here, we investigated the ROS accumulation and GSH depletion in HCC cells, and our results demonstrated that iberberin treatment could enhance oxidative stress in Huh7, Huh7.5.1 and SNU739 cells in a dose-dependent manner, as evidenced by the increase in the production of ROS and simultaneously depletion of GSH (Figure 9). Thus, it was suggested that iberberin caused DNA damage and G2/M checkpoint mediated by ROS generation.

In summary, the present study confirmed that iberberin could induce DNA damage and G2/M arrest through ROS generation and promote mitochondrial-related apoptosis, ultimately exerting anti-HCC activities (Figure 10).

## 4 Discussion

There is growing evidence from encouraging *in vitro* and *in vivo* animal models that ITCs have multiple biological activities including plant defense and benefits to human health (antioxidant, antimicrobial and anticarcinogenic properties) (Jain et al., 2019; Chuang et al., 2020; Li et al., 2021; Lohning et al., 2021; Dixit et al., 2022). ITCs have been found to exert anticarcinogenic activity in diverse cancers, such as lung cancer, breast cancer, prostate cancer and bladder cancer (Psurki et al., 2019; Zheng et al., 2019; Justin et al., 2020; Nguyen et al., 2020). Accumulating studies *in vitro* and *in vivo* animal models revealed that ITCs, such as BITC, PEITC and SFN, could inhibit HCC by suppressing cell proliferation, inhibiting cell migration, inducing apoptosis and/or autophagy (Dinh et al., 2021; Haq et al., 2022; Zhang et al., 2022). As a predominant ITC derived from the seeds of oxheart cabbage, iberberin has been proved to have great antineoplastic activity in lung cancer A549 cells and cervical cancer HeLa cells (Wang et al., 2010; Wang et al., 2016). In this study, we dissected the effect of iberberin in human HCC cells *in vitro* and found that iberberin could inhibit cell proliferation, suppress migration and invasion, induce apoptosis, and impair cell cycle progression. In addition, the xenograft tumor assay further verified the antineoplastic roles of iberberin in HCC *in vivo* without obvious toxicity, making it a promising candidate for novel anti-HCC treatments.

Previous studies have reported that ITCs, such as PEITC, BITC and SFN, could trigger a series of mitochondria-related apoptotic responses, which ultimately promote the accumulation of ROS that causes DNA damage to kill cancer cells (Sestili et al., 2010; Huang et al., 2014; Henklewska et al., 2021). Our results showed that

iberberin might also exert its anticarcinogenic activity against HCC through mitochondria-related apoptotic pathway. Decreased MMP mediated by Bax and Bcl-2 was observed in HCC cells after iberberin treatment. In addition, GSEA analysis revealed that genes enriched in the tumor suppressor p53 pathway were activated in HCC cells following iberberin exposure, which could also directly affect MMP (Noutsopoulos et al., 2010). Mitochondria-related apoptotic responses induced by iberberin, including decrease of MMP, increase of Bax expression and decrease of Bcl-2 expression, could further promote the enhancement of MOMP, which further activates Caspase-dependent apoptosis and promotes ROS generation that causes DNA damage (Estaquier et al., 2012).

Accumulating evidence from encouraging *in vitro* and *in vivo* animal models has demonstrated that ROS induces DNA damage, checkpoint responses, and apoptosis in diverse cancers (Barzilai and Yamamoto, 2004; Guachalla and Rudolph, 2010; Guo et al., 2014; Sadiq, 2023). In some cases, ITCs cause cell cycle arrest via the enhanced ROS accumulation. For example, a recent study showed that SFN, iberin and Alysin induced the intracellular ROS generation that led to S and G2/M phase arrest, and ultimately blocked proliferation in HepG2 cells (Ye et al., 2020). In the present study, we also found that iberberin could induce DNA damage and cause G2/M cell cycle arrest in a ROS-dependent manner in HCC, which was further supported by the enrichment gene sets for the activated G2/M checkpoint and DNA repair from GSEA.

In summary, our study demonstrates that iberberin induces the production of ROS, causing DNA damage and subsequent G2/M cell cycle arrest, and activates mitochondrial-related apoptotic responses, which in turn induce growth inhibitory and apoptosis in HCC. Furthermore, our results suggests that G2/M DNA damage checkpoint might be a key tumor suppressor checkpoint and critical for the anti-cancer activity of iberberin. Our data indicate that iberberin is a promising biotherapeutic agent against HCC. In order to maximize the potential clinical application of iberberin, more experimental support from *in vivo* and *in vitro* studies are urgently needed in future.

## Data availability statement

The original contributions presented in the study are publicly available. This data can be found here: [<http://www.ncbi.nlm.nih.gov/bioproject/1048638>]. Accession number: PRJNA1048638].

## Ethics statement

Ethical approval was not required for the studies on humans in accordance with the local legislation and institutional requirements because only commercially available established cell lines were used. The animal study was approved by the

Animal Ethical and Welfare Committee of Wenzhou University. The study was conducted in accordance with the local legislation and institutional requirements.

## Author contributions

YZ: Data curation, Formal Analysis, Investigation, Visualization, Writing–original draft. JD: Data curation, Formal Analysis, Investigation, Visualization, Writing–original draft. LJ: Data curation, Investigation, Validation, Writing–original draft. LP: Data curation, Investigation, Writing–original draft. XY: Conceptualization, Funding acquisition, Methodology, Project administration, Resources, Supervision, Writing–review and editing. SL: Conceptualization, Funding acquisition, Methodology, Project administration, Resources, Supervision, Writing–review and editing.

## Funding

The author(s) declare financial support was received for the research, authorship, and/or publication of this article. This research was funded by the International Cooperation Projects of National Key R&D Program of China [2022YFE0108300], the Basic Scientific Research Projects of Wenzhou [N20210003] and the Master's Innovation Foundation of Wenzhou University [3162023003045].

## Conflict of interest

The authors declare that the research was conducted in the absence of any commercial or financial relationships that could be construed as a potential conflict of interest.

## Publisher's note

All claims expressed in this article are solely those of the authors and do not necessarily represent those of their affiliated organizations, or those of the publisher, the editors and the reviewers. Any product that may be evaluated in this article, or claim that may be made by its manufacturer, is not guaranteed or endorsed by the publisher.

## Supplementary material

The Supplementary Material for this article can be found online at: <https://www.frontiersin.org/articles/10.3389/fphar.2023.1326346/full#supplementary-material>

## References

- Akinyemiju, T., Abera, S., Ahmed, M., Alam, N., Alemayohu, M. A., Allen, C., et al. (2017). The burden of primary liver cancer and underlying etiologies from 1990 to 2015 at the global, regional, and national level: results from the global burden of disease study 2015. *JAMA Oncol.* 3, 1683–1691. doi:10.1001/jamaoncol.2017.3055
- Arfin, S., Jha, N. K., Jha, S. K., Kesari, K. K., Ruokolainen, J., Roychoudhury, S., et al. (2021). Oxidative stress in cancer cell metabolism. *Antioxidants* 10, 642. doi:10.3390/antiox10050642
- Barzilai, A., and Yamamoto, K. I. (2004). DNA damage responses to oxidative stress. *DNA Repair* 3, 1109–1115. doi:10.1016/j.dnarep.2004.03.002



- Boldry, E. J., Yuan, J. M., Carmella, S. G., Wang, R., Tessier, K., Hatsukami, D. K., et al. (2020). Effects of 2-phenethyl isothiocyanate on metabolism of 1,3-butadiene in smokers. *Cancer Prev. Res.* 13, 91–100. doi:10.1158/1940-6207.CAPR-19-0296
- Chuang, W. T., Yen, C. C., Huang, C. S., Chen, H. W., and Lii, C. K. (2020). Benzyl isothiocyanate ameliorates high-fat diet-induced hyperglycemia by enhancing Nrf2-dependent antioxidant defense-mediated IRS-1/AKT/TBC1D1 signaling and GLUT4 expression in skeletal muscle. *J. Agric. Food Chem.* 68, 15228–15238. doi:10.1021/acs.jafc.0c06269
- Dinh, T. N., Parat, M. O., Ong, Y. S., and Khaw, K. Y. (2021). Anticancer activities of dietary benzyl isothiocyanate: a comprehensive review. *Pharmacol. Res.* 169, 105666. doi:10.1016/j.phrs.2021.105666
- Dixit, S., Widemann, E., Bensoussan, N., Salehipourshirazi, G., Bruinsma, K., Milojevic, M., et al. (2022).  $\beta$ -Cyanoolanine synthase protects mitochondria against arabidopsis defenses. *Plant Physiol.* 189, 1961–1975. doi:10.1093/plphys/kiac147
- Dong, H., Wang, M., Chang, C., Sun, M., Yang, F., Li, L., et al. (2020). Erianin inhibits the oncogenic properties of hepatocellular carcinoma via inducing DNA damage and aberrant mitosis. *Biochem. Pharmacol.* 182, 114266. doi:10.1016/j.bcp.2020.114266
- Engeland, K. (2022). Cell cycle regulation: p53-p21-RB signaling. *Cell Death Differ.* 29, 946–960. doi:10.1038/s41418-022-00988-z
- Estaquier, J., Vallette, F., Vayssiere, J. L., and Mignotte, B. (2012). The mitochondrial pathways of apoptosis. *Adv. Exp. Med. Biol.* 942, 157–183. doi:10.1007/978-94-007-2869-1\_7
- Estes, C., Razavi, H., Loomba, R., Younossi, Z., and Sanyal, A. J. (2018). Modeling the epidemic of nonalcoholic fatty liver disease demonstrates an exponential increase in burden of disease. *Hepatology* 67, 123–133. doi:10.1002/hep.29466
- Fontana, F., Raimondi, M., Marzagalli, M., Di Domizio, A., and Limonta, P. (2020). The emerging role of paraptosis in tumor cell biology: perspectives for cancer prevention and therapy with natural compounds. *Biochim. Biophys. Acta Rev. Cancer* 1873, 188338. doi:10.1016/j.bbcan.2020.188338
- Guachalla, L. M., and Rudolph, K. L. (2010). ROS induced DNA damage and checkpoint responses influences on aging? *Cell Cycle* 9, 4058–4060. doi:10.4161/cc.9.20.13577
- Guo, J., Wu, G., Bao, J., Hao, W., Lu, J., and Chen, X. (2014). Cucurbitacin B induced ATM-mediated DNA damage causes G2/M cell cycle arrest in a ROS-dependent manner. *PLoS One* 9, e88140. doi:10.1371/journal.pone.0088140
- Haq, I. U., Khan, S., Awan, K. A., and Iqbal, M. J. (2022). Sulforaphane as a potential remedy against cancer: comprehensive mechanistic review. *J. Food Biochem.* 46, e13886. doi:10.1111/jfbc.13886
- Helton, E. S., and Chen, X. (2007). P53 modulation of the DNA damage response. *J. Cell. Biochem.* 100, 883–896. doi:10.1002/jcb.21091
- Henkleska, M., Pawlak, A., Li, R. F., Yi, J., Zbyryt, I., and Obminska Mrukowicz, B. (2021). Benzyl isothiocyanate, a vegetable-derived compound, induces apoptosis via ROS accumulation and DNA damage in canine lymphoma and leukemia cells. *Int. J. Mol. Sci.* 22, 11772. doi:10.3390/ijms221111772
- Huang, S. H., Hsu, M. H., Hsu, S. C., Yang, J. S., Huang, W. W., Huang, A. C., et al. (2014). Phenethyl isothiocyanate triggers apoptosis in human malignant melanoma A375.S2 cells through reactive oxygen species and the mitochondria-dependent pathways. *Hum. Exp. Toxicol.* 33, 270–283. doi:10.1177/0960327113491508
- Jain, M. K., Rich, N. E., Ahn, C., Turner, B. J., Sanders, J. M., Adamson, B., et al. (2019). Evaluation of a multifaceted intervention to reduce health disparities in hepatitis C screening: a pre-post analysis. *Hepatology* 70, 40–50. doi:10.1002/hep.30638
- Justin, S., Rutz, J., Maxeiner, S., Chun, F. K. H., Juengel, E., and Blaheta, R. A. (2020). Bladder cancer metastasis induced by chronic everolimus application can be counteracted by sulforaphane *in vitro*. *Int. J. Mol. Sci.* 21, 5582. doi:10.3390/ijms211155582
- Kaufmann, S. H., Mesner, P. W., Samejima, K., Toné, S., and Earnshaw, W. C. (2000). Detection of DNA cleavage in apoptotic cells. *Methods Enzym. Apoptosis* 322, 3–15. doi:10.1016/S0076-6879(00)22003-X
- Kawase, T., Ichikawa, H., Ohta, T., Nozaki, N., Tashiro, F., Ohki, R., et al. (2008). p53 target gene AEN is a nuclear exonuclease required for p53-dependent apoptosis. *Oncogene* 27, 3797–3810. doi:10.1038/onc.2008.32
- Kubczak, M., Szustka, A., and Rogalińska, M. (2021). Molecular targets of natural compounds with anti-cancer properties. *Int. J. Mol. Sci.* 22, 13659. doi:10.3390/ijms222413659
- Li, P., Zhao, Y., Wang, C., and Zhu, H. (2021). Antibacterial activity and main action pathway of benzyl isothiocyanate extracted from papaya seeds. *J. Food Sci.* 86, 169–176. doi:10.1111/1750-3841.15539
- Lin, C. W., Lin, C. C., Mo, L. R., Chang, C. Y., Perng, D. S., Hsu, C. C., et al. (2013). Heavy alcohol consumption increases the incidence of hepatocellular carcinoma in hepatitis B virus-related cirrhosis. *J. Hepatol.* 58, 730–735. doi:10.1016/j.jhep.2012.11.045
- Liu, X., Fu, R., Pan, Y., Meza Sosa, K. F., Zhang, Z., and Lieberman, J. (2018). PNP1 release from mitochondria during apoptosis triggers decay of poly(A) RNAs. *Cell* 174, 187–201. doi:10.1016/j.cell.2018.04.017
- Llovet, J. M., Kelley, R. K., Villanueva, A., Singal, A. G., Pikarsky, E., Roayaie, S., et al. (2021). Hepatocellular carcinoma. *Nat. Rev. Dis. Prim.* 7, 6. doi:10.1038/s41572-020-00240-3
- Llovet, J. M., Zucman Rossi, J., Pikarsky, E., Sangro, B., Schwartz, M., Sherman, M., et al. (2016). Hepatocellular carcinoma. *Nat. Rev. Dis. Prim.* 2, 16018. doi:10.1038/nrdp.2016.18
- Lohning, A., Kidachi, Y., Kamiie, K., Sasaki, K., Ryoyama, K., and Yamaguchi, H. (2021). 6-(methylsulfinyl)hexyl isothiocyanate (6-MITC) from *Wasabia japonica* alleviates inflammatory bowel disease (IBD) by potential inhibition of glycogen synthase kinase 3 beta (GSK-3 $\beta$ ). *Eur. J. Med. Chem.* 216, 113250. doi:10.1016/j.ejmech.2021.113250
- Nambiar, D. M., Kumari, J., Arya, G. C., Singh, A. K., and Bisht, N. C. (2020). A cell suspension based uptake method to study high affinity glucosinolate transporters. *Plant Methods* 16, 75. doi:10.1186/s13007-020-00618-0
- Nguyen, Y. T. K., Moon, J. Y., Ediriweera, M. K., and Cho, S. K. (2020). Phenethyl isothiocyanate suppresses stemness in the chemo- and radio-resistant triple-negative breast cancer cell line MDA-MB-231/IR via downregulation of metadherin. *Cancers* 12, 268. doi:10.3390/cancers12020268
- Noutsopoulos, D., Markopoulos, G., Vartholomatos, G., Kolettas, E., Kolaitis, N., and Tzavaras, T. (2010). VL30 retrotransposition signals activation of a caspase-independent and p53-dependent death pathway associated with mitochondrial and lysosomal damage. *Cell Res.* 20, 553–562. doi:10.1038/cr.2010.48
- Psurski, M., Filip Psurska, B., Cuprych, M., Wietrzyk, J., and Oleksyszyn, J. (2019). 3,4-dimethoxybenzyl isothiocyanate enhances doxorubicin efficacy in LoVoDX doxorubicin-resistant colon cancer and attenuates its toxicity *in vivo*. *Life Sci.* 231, 116530. doi:10.1016/j.lfs.2019.06.005
- Rakariyatham, K., Yang, X., Gao, Z., Song, M., Han, Y., Chen, X., et al. (2019). Synergistic chemopreventive effect of allyl isothiocyanate and sulforaphane on non-small cell lung carcinoma cells. *Food Funct.* 10, 893–902. doi:10.1039/C8FO01914B
- Rekha, K., Venkidasamy, B., Govindasamy, R., Neralla, M., and Thiruvengadam, M. (2022). Isothiocyanates (AITC and BITC) bioactive molecules: therapeutic potential for oral cancer. *Oral Oncol.* 133, 106060. doi:10.1016/j.oraloncology.2022.106060
- Sadiq, I. Z. (2023). Free radicals and oxidative stress: signaling mechanisms, redox basis for human diseases, and cell cycle regulation. *Curr. Mol. Med.* 23, 13–35. doi:10.2174/1566524022666211222161637
- Sestili, P., Paolillo, M., Lenzi, M., Colombo, E., Vallorani, L., Casadei, L., et al. (2010). Sulforaphane induces DNA single strand breaks in cultured human cells. *Mutat. Res. Fundam. Mol. Mech. Mutagen.* 689, 65–73. doi:10.1016/j.mrfmmm.2010.05.003
- Siegel, R. L., Miller, K. D., Fuchs, H. E., and Jemal, A. (2021). Cancer statistics, 2021. *CA Cancer J. Clin.* 71, 7–33. doi:10.3322/caac.21654
- Singh, S., Singh, P. P., Roberts, L. R., and Sanchez, W. (2014). Chemopreventive strategies in hepatocellular carcinoma. *Nat. Rev. Gastroenterol. Hepatol.* 11, 45–54. doi:10.1038/nrgastro.2013.143
- Sung, H., Ferlay, J., Siegel, R. L., Laversanne, M., Soerjomataram, I., Jemal, A., et al. (2021). Global cancer statistics 2020: globocan estimates of incidence and mortality worldwide for 36 cancers in 185 countries. *CA A Cancer J. Clin.* 71, 209–249. doi:10.3322/caac.21660
- Tewari, D., Patni, P., Bishayee, A., Sah, A. N., and Bishayee, A. (2022). Natural products targeting the PI3K-AKT-mTOR signaling pathway in cancer: a novel therapeutic strategy. *Semin. Cancer Biol.* 80, 1–17. doi:10.1016/j.semcancer.2019.12.008
- Trinchet, J. C., Bourcier, V., Chaffaut, C., Ait Ahmed, M., Allam, S., Marcellin, P., et al. (2015). Complications and competing risks of death in compensated viral cirrhosis (ANRS CO12 CirVir prospective cohort). *Hepatology* 62, 737–750. doi:10.1002/hep.27743
- Wang, N., Shen, L., Qiu, S., Wang, X., Wang, K., Hao, J., et al. (2010). Analysis of the isothiocyanates present in three Chinese Brassica vegetable seeds and their potential anticancer bioactivities. *Eur. Food Res. Technol.* 231, 951–958. doi:10.1007/s00217-010-1348-x
- Wang, N., Wang, W., Liu, C., Jin, J., Shao, B., and Shen, L. (2016). Inhibition of growth and induction of apoptosis in A549 cells by compounds from oxheart cabbage extract: bioactive compounds from oxheart cabbage extract. *J. Sci. Food Agric.* 96, 3813–3820. doi:10.1002/jsfa.7575
- Ye, Z., Zheng, M., Zeng, Y., Wei, S., Wang, Y., Lin, Z., et al. (2020). Bioinformatics analysis reveals an association between cancer cell stemness, gene mutations, and the immune microenvironment in stomach adenocarcinoma. *Front. Genet.* 11, 595477. doi:10.3389/fgene.2020.595477
- Zhang, Y., Huang, H., Jin, L., and Lin, S. (2022). Anticarcinogenic effects of isothiocyanates on hepatocellular carcinoma. *Int. J. Mol. Sci.* 23, 13834. doi:10.3390/ijms232213834
- Zheng, Z., Lin, K., Hu, Y., Zhou, Y., Ding, X., Wang, Y., et al. (2019). Sulforaphane metabolites inhibit migration and invasion via microtubule-mediated Claudins dysfunction or inhibition of autolysosome formation in human non-small cell lung cancer cells. *Cell Death Dis.* 10, 259. doi:10.1038/s41419-019-1489-1